Elsevier Editorial System(tm) for European Journal of Pharmaceutics and Biopharmaceutics
Manuscript Draft

Manuscript Number: EJPB-D-14-00244R1

Title: Biodistribution of nanostructured lipid carriers: a tomographic study

Article Type: Research Paper

Keywords: nanostructured lipid carriers, biodistribution, 99mTc imaging agents, Cryo Transmission Electron Microscopy (cryo-TEM), Photon Correlation Spectroscopy (PCS); single photon emission computed tomography (SPECT)

Corresponding Author: Prof. Claudio Nastruzzi,

Corresponding Author's Institution: University of Ferrara

First Author: Elisabetta Esposito, PhD

Order of Authors: Elisabetta Esposito, PhD; Alessandra Boschi; Laura Ravani; Rita Cortesi; Markus Drechsler; Paolo Mariani; Silvia Moscatelli; Catia Contado; Giovanni Di Domenico; Claudio Nastruzzi; Melchiore Giganti; Licia Uccelli

Manuscript Region of Origin: ITALY

Abstract: This study describes the preparation, characterization, and biodistribution of radiolabeled nanostructured lipid carriers (NLC) especially designed for in vivo tomographic study.A preliminary formulative study was conducted in order to incorporate 99mTc based tracer in NLCs. At this aim a 99mTc complex containing a terminal 99mTc≡N multiple bond ([99mTc]N-DBODC2) has been synthetized and included in NLCs produced by a stirring and ultrasonication method.The morphological and dimensional characteristics of the produced NLCs have been accurately investigated by a number of specific techniques, including: cryogenic transmission electron microscopy, x-ray, photon correlation spectroscopy and sedimentation field flow fractionation. The obtained NLCs were employed for achieving in vivo tomographic images of the rat body by small-animal SPECT scanner that enabled the investigation of NLC biodistribution after intraperitoneal, intravenous, intranasal and oral administration. NLC production protocol allowed to firmly encapsulate the radiotracer within the nanoparticles. In vivo studies evidenced that NLC remained stable in vivo, suggesting their suitability as controlled release system for drugs and radiochemical for therapeutic and diagnostic purposes.Moreover the high resolution images obtained by the SPECT technique allowed to detect NLC presence in brown fat tissue, suggesting NLC therapeutic application for treating human obesity and related metabolic disorders.

Cover Letter

Ferrara, 17 April 2014

Dear Prof. A. Goepferich,

Enclosed please find a manuscript to be submitted for possible publication on “European Journal of Pharmaceutics and Biopharmaceutics”.

The manuscript is entitled:

"Biodistribution of nanostructured lipid carriers: a tomographic study" by Elisabetta Esposito, Alessandra Boschi, Laura Ravani, Rita Cortesi, Markus Drechsler, Paolo Mariani, Silvia Moscatelli, Catia Contado, Giovanni Di Domenico, Claudio Nastruzzi, Melchiore Giganti, Licia Uccelli.

The object of the paper is the preparation, characterization, and biodistribution of radiolabelled nanostructured lipid carriers (NLC) especially designed for in vivo tomographic study. The novelties of the study are (a) the method of inclusion of a ^{99m}Tc complex containing a terminal ^{99m}Tc≡N multiple bond ([^{99m}Tc]N-DBODC$_2$) in NLCs (b) the in vivo tomographic comparation of NLC biodistribution by different administration routes using small-animal SPECT scanner.

The manuscript is original, unpublished, it is not under consideration for publication elsewhere, and all authors have read and approved the text and consent to its publication.

I thank you in advance for consideration.

Best regards

Prof Claudio Nastruzzi

***Response to Reviewers**

We thank the Editor and the Reviewer for their positive and insightful comments on our manuscript. We have thoroughly revised the manuscript to accomplish with the Reviewer suggestions.

In reply to Reviewer #1

Q 1.) The stability of the association of the label and the particles has to be proven. Otherwise it could be that the label only is imaged and not the labeled particles. Indeed, the authors give two references which underline that the label itself should be distributed in a different way but I think this is not enough of a proof.

A 1.) In order to accomplish to the reviewer's comment, a stability study has been performed in vitro incubating ^{99m}Tc-NLC in rat serum, demonstrating that the ^{99m}Tc-$DBODC_2$ remained stably associated to NLC. The details of the experiments have been included in the methods section, while the results have been reported in a new figure (new Figure 6) and in the results section.

Q 2.) What is the detection limit of the method? Would it make sense to compare the data with e.g. blood values etc. for some selected samples?

A 2.) As requested by the reviewer, the detection limit for SPECT (1.34 MBq) has been included in the results section.

Q 3.) Why are the particles so extensively characterized with two different methods? The particles seem to have a broad size distribution anyway and particle size does not play any role later in the manuscript.

A 3.) Particle characterization, especially in term of size and size distribution, represents a highly relevant aspect for quality control, stability evaluation and biological fate of any particulate delivery system. Physical properties such as morphology, size and size distribution of nanoparticles indeed heavily affect their biological activity, biodistribution and toxicity. Meanwhile, due to the complex and dynamic nature of nanoparticles and to the different principles at the base of characterization techniques, the obtained size distribution strongly depends on the employed method. For this reason, in our manuscript, the combination of complementary measurement techniques was employed, in order to overcome the impairment of a single technique.

Size distribution analyses allowed to verify the suitability of the particles for in vivo administration and in this respect, a new paragraph and reference have been added to the manuscript to underline this importance.

With respect to the reviewer comment about the "broad size distribution" of particles, we would like to underline that the overall plot size distribution (reported in Fig. 2) could appear broad, by looking to the x-scale of the graphs, but it should be considered that the plots highlight that the majority of the particles have actually a narrow distribution.

In addition, photon correlation spectroscopy determination (reported in Table 3) confirmed that particles are characterized by a narrow size distribution (P.I. lower than 0.25), especially in the case of ^{99m}Tc-NLC (70%<150 nm) that were later employed for in vivo studies.

Q 4.) The style of the manuscript is poor. For example: Certain passages are hard to read because abbreviations were not introduced, methods are described in the results section. The introduction is far too long, too general and not brought to the point. In contrast, the interesting in vivo results are described only in few sentences. The manuscript should be completely overhauled with this respect.

A 4.) As suggested by the reviewer, the style of manuscript has been thoroughly revised.

a) The introduction has been shortened and changed.

b) Abbreviations have been introduced in the new Table 2 that includes batch identification codes and composition of the produced nanoparticles.

c) The result section was rewritten, moving the description of the methods to the experimental section. Two new figures (Fig. 6 and Fig. 8) have been inserted and commented.

d) The description and the comments of the in vivo results have been implemented.

e) Finally the conclusions have been rewritten.

Q 5.) Other similar studies are already available. Hence, the novelty of this work should be presented in a much better way.

A 5.) The novelty of the work has been highlighted in the results and discussion and conclusions sections. In particular it has been underlined that

a) we have employed SPECT as a new technique to study lipid nanoparticle biodistribution, resulting in very higher resolution images with respect to many papers based on different techniques.

b) we have developed a production procedure able to firmly encapsulate the radiotracer within the nanoparticle matrix while other papers describe a tracer association after nanoparticle production, without controlling stability of tracer-nanoparticle complex.
c) we have selected ^{99m}Tc as radiotracer of nanoparticle because this molecule has a particular tropism for myocardial tissue. The absence of radioactivity in the heart indicated that ^{99m}Tc was not “free” and was instead associated to NLC.
d) the importance of NLC targeting to brown fat tissue and its possible implications for obesity therapies.

Hoping the manuscript is now suitable for publication in European Journal of Pharmaceutics and Biopharmaceutics, I send my very best regards

*Graphical abstract (for review)

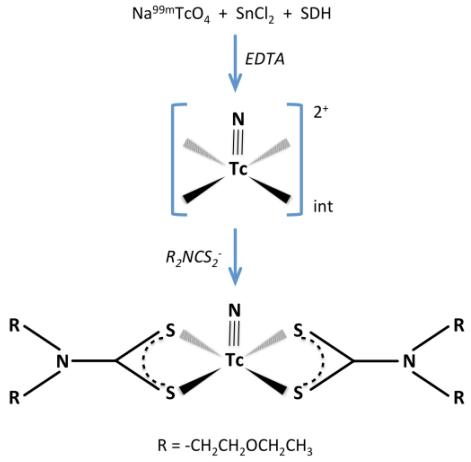

99mTc complex

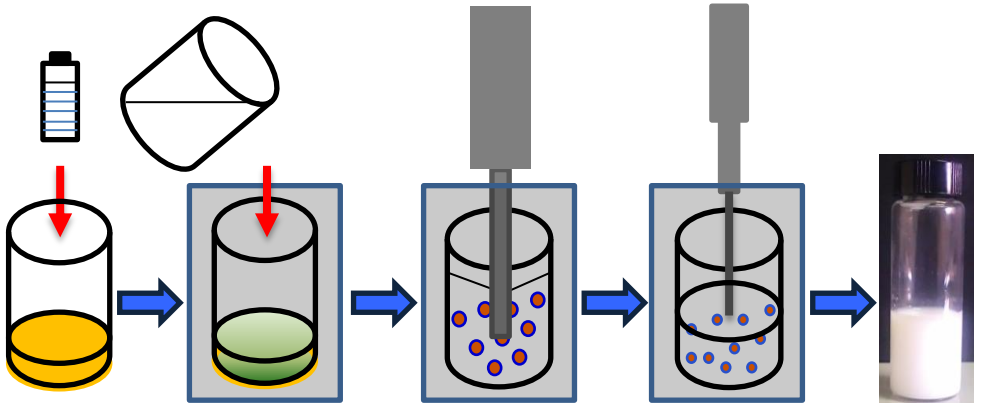

lipid phase

O/W emulsion

99mTc-NLC

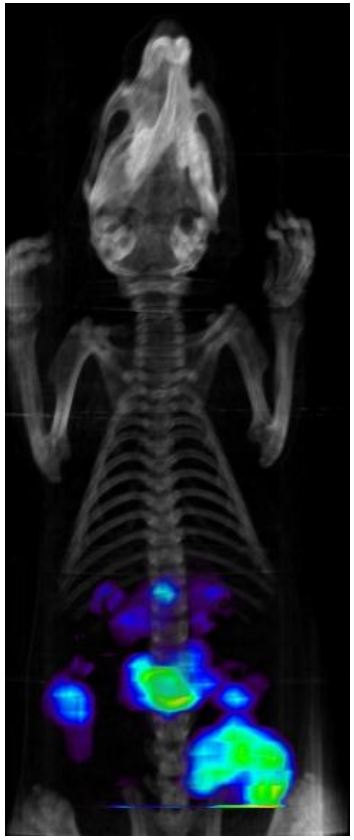

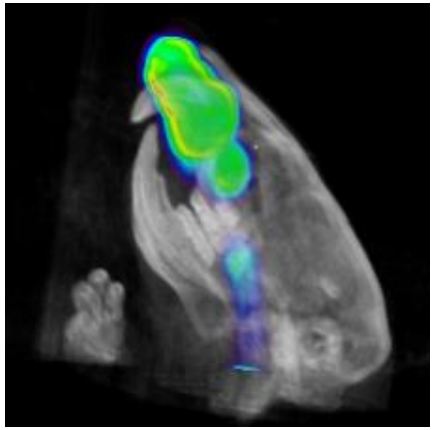

i.p., i.v., per os, i.n. routes

small-animal YAP-(S)-PET scanner

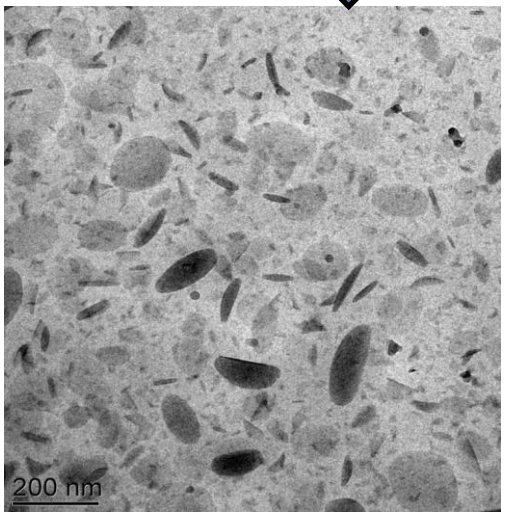

- Radiolabeled lipid nanoparticles for biodistribution study are obtained
- ^{99m}Tc-DBODC$_2$ included in nanoparticle does not affect their morphology and dimension
- SPECT technique evaluates nanoparticle biodistribution, by high-quality images
- It was possible to detect the lipid nanoparticle presence in brown fat tissue.

Biodistribution of nanostructured lipid carriers: a tomographic study

Elisabetta Esposito[a], Alessandra Boschi[b], Laura Ravani[a], Rita Cortesi[a], Markus Drechsler[c], Paolo Mariani[d], Silvia Moscatelli[d], Catia Contado[e], Giovanni Di Domenico[f], Claudio Nastruzzi[a*], Melchiore Giganti[b], Licia Uccelli[b]

[a]*Department of Life Sciences and Biotechnology, University of Ferrara, I-44121 Ferrara, Italy*
[b]*Department of Morphology, Surgery and Experimental Medicine, University of Ferrara, I-44121 Ferrara, Italy*
[c]*BIMF / Soft Matter Electronmicroscopy , University of Bayreuth, Germany*
[d]*Department of Life and Environmental Sciences and CNISM, Università Politecnica delle Marche, I-60100 Ancona, Italy*
[e]*Department of Chemistry, University of Ferrara, I-44121 Ferrara, Italy*
[f]*Department of Physic and Earth Science, University of Ferrara, I-44121 Ferrara, Italy*

*Correspondence to: Prof. Claudio Nastruzzi
Department of Life Sciences and Biotechnology
Via Fossato di Mortara, 19
I-44121 Ferrara, Italy
Tel. +39/0532/455348
Fax. +39/0532/455953
e-mail nas@unife.it

ABSTRACT

This study describes the preparation, characterization, and biodistribution of radiolabelled nanostructured lipid carriers (NLC) especially designed for in vivo tomographic study.

A preliminary formulative study was conducted in order to incorporate ^{99m}Tc based tracer in NLCs. At this aim a ^{99m}Tc complex containing a terminal ^{99m}Tc≡N multiple bond ([^{99m}Tc]N-DBODC$_2$) has been synthetized and included in NLCs produced by a stirring and ultrasonication method.

The morphological and dimensional characteristics of the produced NLCs have been accurately investigated by a number of specific techniques, including: cryogenic transmission electron microscopy, x-ray, photon correlation spectroscopy and sedimentation field flow fractionation. The obtained NLCs were employed for achieving in vivo tomographic images of the rat body by small-animal SPECT scanner that enabled the investigation of NLC biodistribution after intraperitoneal, intravenous, intranasal and oral administration. NLC production protocol allowed to firmly encapsulate the radiotracer within the nanoparticles. In vivo studies evidenced that NLC remained stable in vivo, suggesting their suitability as controlled release system for drugs and radiochemical for therapeutic and diagnostic purposes.

Moreover the high resolution images obtained by the SPECT technique allowed to detect NLC presence in brown fat tissue, suggesting NLC therapeutic application for treating human obesity and related metabolic disorders.

Keywords:

nanostructured lipid carriers, biodistribution, ^{99m}Tc imaging agents, Cryo Transmission Electron Microscopy (cryo-TEM), Photon Correlation Spectroscopy (PCS); single photon emission computed tomography (SPECT).

Abbreviations:

C-NLC: conventional nanostructured lipid carriers, prepared without the addition of EtOH; EtOH-NLC: nanostructured lipid carrier, prepared with the addition of plain EtOH; ^{99m}Tc-NLC: radiolabeled nanostructured lipid carrier, prepared with the addition of EtOH containing the [^{99m}Tc]N-DBODC$_2$ tracer; Cryo Transmission Electron Microscopy: cryo-TEM, Photon Correlation Spectroscopy: PCS; Sedimentation Field Flow fractionation: SdFFF; polydispersity index: P.I.; single photon emission computed tomography: SPECT; lipid phase: LP; water phase: WP; Stannous chloride dihydrate, succinic dihydrazide: SDH; ethylenediaminotetraacetic acid: EDTA; sodium salt of the bis(dithiocarbamate) ligand: DBODC; glutathione: GSH; radiochemical purity: RCP; thin-layer chromatography: TLC; ethanol: EtOH; corpus adiposum nuchae: CAN intraperitoneal: i.p.; intravenous: i.v.; intranasal i.n.; oral: per os.

1. Introduction

The understanding of the in vivo absorption, distribution, metabolism, and excretion of nanoparticle based drug delivery systems represents a keystone to assure the efficacy, safety and reliability of clinically oriented formulation [1].

In recent years the pharmaceutical research panorama has been highly showered by nanoparticle based studies; a number of nanoparticles made of different excipients (e.g. polymers or lipids) have been indeed proposed for the treatment of numerous pathologies [2-5].

In particular, lipid-based nanoparticles have attracted a large attention as possible alternatives to polymeric ones due to their highly biocompatible and biodegradable natural components [6]. The lipid excipients used for lipid nanoparticles production have indeed well-established safety profiles and are largely employed in FDA approved products [7,8].

In addition, due to the physicochemical properties of lipids (i.e. the low melting temperature), lipid based nanoparticles can be easily obtained by direct emulsification of the molten lipids and subsequent recrystallization, avoiding the use of potentially toxic solvents that are commonly required for the preparation of polymeric nanoparticles.

Among the different types of lipid-based nanoparticles, nanostructured lipid carriers (NLC) constituted of blends of lipids in solid and liquid state (e.g. oils dispersed in triglycerides) can be thought as the last generation [9]. During production, after melting and re-crystallization of the solid constituents, the differently structured lipids lead to a highly disordered, imperfect lipid matrix that offers large molecular cavities for drug molecules [9,10] assuring high drug loading capacity and maintaining drug stability during storage [11-13].

Taken together, the above mentioned aspects make NLC ideal tools for medical applications [9,10,14].

One crucial point about the in vivo use of nanoparticles and in particular of NLC is the study of their in vivo biodistribution. In spite of a large amount of knowledge about the physicochemical characteristics of NLC and their in vitro performances, relatively less studies describe their in vivo biodistribution, organ accumulation and elimination [15-18].

In order to perform biodistribution studies, different nuclear medicine techniques have been developed based on emission techniques in which the source of electromagnetic radiation is a radioisotope that is distributed within the body of the patient [19]. In particular

positron emission tomography (PET) has been developed as noninvasive, nuclear imaging technique for visualizing deep tissues with a high sensitivity.

Nonetheless PET technique is unfortunately limited to those radioisotopes that decay by emitting a positron, for this reason valuable alternatives, such as single photon emission computed tomography (SPECT) technology, have been considered [20].

In particular Di Domenico and colleagues have constructed the high resolution YAP-(S)PET small animal integrated PET-SPECT upgraded with a computed tomography (CT) [21,22]. The instrument allows to perform in vivo molecular and genomic imaging studies on small animals (e.g. mice and rats) with ^{99m}Tc labeled radiotracers, obtaining at the same time morphological information needed to correct attenuation and to restrict more precisely the region under investigation [19].

In this context, the current paper concerns a novel method to study the biodistribution of lipid nanoparticles.

In particular the first part of the investigation describes a formulation study aimed to radiolabel NLCs by the inclusion of a positron emitter, [^{99m}Tc]N-DBODC$_2$, into the lipid constituents. A suitable strategy to directly incorporate the ^{99m}Tc complex into NLC has been selected and the influence of the complex inclusion on NLC dimensional distribution, morphology and inner structure has been investigated.

In the second part, the biodistribution of radiolabeled NLC administered in rats is explored. In particular NLC have been alternatively administered by intraperitoneal (i.p.), intravenous (i.v.), intranasal (i.n.) or oral (per os) routes, afterwards in vivo tomographic images of the rat body were obtained by use of the YAP-(S)-PET small animal scanner prototype [20,21].

2. Materials and Methods

2.1. Materials

Poloxamer 188, a nonionic tri-block copolymer composed of a central hydrophobic chain of polyoxypropylene (poly(propylene oxide)) flanked by two hydrophilic chains of polyoxyethylene (poly(ethylene oxide)), was a gift of BASF ChemTrade GmbH (Burgbernheim, Germany). Tristearin, stearic triglyceride (tristearin) was provided by Fluka (Buchs-Swiss). Miglyol 812N, caprylic/capric triglycerides (miglyol) was a gift of Cremer Oleo Division (Witten, Germany). The ligand N, N'-bis(ethoxyethyl)dithiocarbamato sodium salt (DBODC) was purchased from Alchemy, Altedo, Italy. Stannous chloride dihydrate, succinic dihydrazide (SDH), and ethylenediaminotetraacetic acid (EDTA) were obtained from Sigma-Aldrich, Milan, Italy. In all procedures, ethanol (EtOH), water and saline suitable for injection were employed. Before use, Sep-Pak cartridges (Waters) were washed with 5.0 mL of sterile water and then steam sterilized. ^{99m}Tc was obtained, as [^{99m}Tc]pertechnetate ion, from a generator ^{99}Mo/^{99m}Tc (Drytec GE, Helthcare, UK).

2.2. Production of NLCs

NLCs were prepared by stirring followed by ultrasonication [28] in the absence or in the presence of EtOH. Briefly, 0.25 g of lipid mixture or 0.25 g of lipid mixture plus 1 mL of EtOH, were melted and left at 75°C for 20 min. The lipid mixture was constituted of tristearin/miglyol 2:1 w/w (lipid phase, LP). To the melted LP, 4.75 mL of an aqueous poloxamer 188 solution (water phase, WP) (2.5 %, w/w) was added. The two phase system was then stirred at 15,000 rpm, at 80°C for 1 min, using a high-speed stirrer (Ultra Turrax T25, IKA-Werke GmbH & Co. KG, Staufen, Germany). The emulsion was then subjected to ultrasonication (Microson TM, Ultrasonic cell Disruptor) at 6.75 kHz for 15 min and then cooled down to room temperature by placing it in a water bath at 25 °C. After preparation, NLCs were stored at room temperature.

2.3. Preparation of [^{99m}Tc] N-DBODC$_2$

In the first step, generator-eluted [^{99m}Tc][TcO_4]$^-$ was mixed with SDH as a donor of nitride nitrogen atoms (N^{3-}), in the presence of Sn^{2+} ions as reducing agent. In particular

$Na^{99m}TcO_4$ (2.0-4.0 GBq) was added to a vial containing 5.0 mg of SDH, 5.0 mg of EDTA, 0.10 mg of $SnCl_2.2H_2O$ dissolved in 0.10 mL of saline plus 1.0 mL of EtOH. The resulting mixture, containing nitride technetium intermediate complexes, whose exact chemical nature is not fully determined, was allowed to stand at room temperature for 30 min. Thereafter, 250 μL of phosphate buffer (100 mM) and 2.0 mg of the sodium salt of the bis(dithiocarbamate) ligand (DBODC) (dissolved in 0.10 mL of saline) were simultaneously added. The vial was kept at room temperature for 15 min. The presence of EDTA in the first step of the reaction was required to prevent the precipitation of the neutral di-substituted $Sn(DBODC)_2$ complex upon the addition of the dithiocarbamate ligand.

Radiochemical purity (RCP) was determined by thin-layer chromatography (TLC). TLC was performed on silica gel plates (Merck) with ethanol:chloroform:toluene:NH_4Ac (0.5 M) (5:3:3:0.5) as the mobile phase (R_f =0.9) and on reversed-phase C18 plates (Merck) with saline:methanol:tetrahydrofuran:glacial acetic acid (2:8:1:1) as the mobile phase (R_f=0.4). Thin-layer chromatograms were analyzed with a Cyclone instrument equipped with a phosphor Imaging screen and OptiQuant image analysis software (Packard Instruments).

The final compound was purified from excess of the reagents using the following procedure. A reversed-phase C18 cartridge (SepPak, Waters) was activated with 5.0 mL of absolute ethanol followed by 5.0 mL of sterile deionized water. The compound [^{99m}Tc]N-$DBODC_2$ was withdrawn from the reaction vial with a 10-mL syringe and passed through the activated cartridge, successively washed with 10 mL of sterile deionized water. Activity was recovered from the cartridge with 1 mL of EtOH, after wasted 400 μL of EtOH.

2.4. Stability of [^{99m}Tc] N-$DBODC_2$

The in vitro stability of [^{99m}Tc]N-$DBODC_2$ was evaluated by monitoring RCP at different times from preparation (15, 30, 60, 120, and 240 min) with the following procedure. After preparation, the compound was purified by the reversed-phase SepPak procedure described above. Thereafter, 100 μL of the collected radioactive eluate were incubated at 37°C with 900 μL of saline, phosphate buffer, rat serum, and NLC. RCP was measured by TLC analysis. Cysteine and glutathione (GSH) are ligands containing sulfur donor atoms that are potentially capable of coordinating the metal fragment [^{99m}Tc]N by substitution of the dithiocarbamate ligand DBODC in [^{99m}Tc]N-$DBODC_2$ compound. Challenge experiments were performed with the following procedure. A 250 μL volume of phosphate buffer (0.2 M pH 7.4), 50 μL of a freshly prepared aqueous solution of L-cysteine (10 mM)

or, alternatively, of GSH (10 mM), and 50 µL of the appropriate complex were placed in a test tube and incubated in a water bath at 37°C. A blank experiment was performed with an equal volume of distilled water in place of the cysteine (or GSH) solution. Aliquots of the resulting solutions were withdrawn at 15, 30, 60, and 120 min and analyzed by TLC.

2.5. Preparation and stability study of radiolabeled NLCs

For the production of radiolabeled NLC (^{99m}Tc-NLC), 1 mL of EtOH containing the purified [^{99m}Tc]N-DBODC$_2$ complex was added to the melted LP. NLC production was conducted by the stirring-ultrasonication procedure previously described, under sterile conditions in biological safety cabinet. After cooling at 25°C, RCP and stability of ^{99m}Tc-NLC were determined by TLC as described in section 2.4. Briefly, 100 µL of radiolabeled NLCs were incubated at 37°C with rat serum and RCP was measured at 1 and 6 hours from the preparation. TLC was performed on reversed-phase C18 plates with saline:methanol:tetrahydrofuran:glacial acetic acid (2:8:1:1) as the mobile phase.

2.6. Photon Correlation Spectroscopy

NLC size analysis was performed by photon correlation spectroscopy (PCS) using a Zetasizer 3000 PCS (Malvern Instr., Malvern, England) equipped with a 5 mW helium neon laser with a wavelength output of 633 nm. Measurements were made at 25 °C at an angle of 90°. Data were interpreted using the “CONTIN” method [23].

2.7. Sedimentation Field Flow Fractionation

A sedimentation field flow fractionation (SdFFF) system (Model S101, FFFractionation, Inc., Salt Lake City, UT, USA), described elsewhere [24], was employed to obtain the particle size distribution (PSD) plots by converting the fractograms [25]. The mobile phase was Milli-Q water (Millipore S.p.A., Vimodrone, Milan, Italy) pumped at 2.0 mL/min. Fifty microliter samples were injected through a 50 µl Rheodyne loop valve.
Fractions were collected every 90 seconds by a Model 2110 fraction collector (Bio Rad laboratories, UK).

2.8. Cryo-Transmission Electron Microscopy

For cryo-transmission electron microscopy (Cryo-TEM) studies, samples were vitrified as previously described [26]. The vitrified specimen was transferred to a Zeiss EM922Omega transmission electron microscope for imaging using a cryoholder (CT3500, Gatan). The temperature of the sample was kept below -175 °C throughout the examination. Specimens were examined with doses of about 1000-2000 e/nm^2 at 200 kV. Images were recorded digitally by a CCD camera (Ultrascan 1000, Gatan) using an image processing system (GMS 1.9 software, Gatan).

2.9. X-ray diffraction

X-ray diffraction experiments were performed using a 3.5kW Philips PW 1830 Xray generator (Philips, Eindhoven, The Netherland) equipped with a home-made Guinier-type focusing camera operating in vacuum with a bent quartz crystal monochromator (λ = 1.54 Å). Diffraction patterns were recorded on a GNR analytical instruments imaging plate system (GNR Analytical Instruments Group, Novara, Italy). Samples were held in a tight vacuum cylindrical cell provided with thin mylar windows. Diffraction data were collected at ambient temperature (25°C), using a Haake F3 thermostat (ThermoHaake, Karlsruhe, Germany) with an accuracy of 0.1°C.

In each experiment, the spacing of the Bragg peaks (one or two in a few cases) observed in the low-angle X-ray diffraction region (Q<0.6 Å-1, being Q the modulus of the scattering vector defined by $Q = 4\pi \sin\theta/\lambda$, where 2θ is the scattering angle) was measured. The peak indexing was performed considering the different symmetries commonly observed in lipid phases [27]. The indexing problem was easy to solve, because in all cases the spacing ratios of the observed Bragg peaks where fully compatible with the 1-dimensional lamellar symmetry (spacing ratios 1: 2 ...). From the averaged spacing of the observed peaks, the unit cell dimension, d, which corresponds to the distance between the mid-plane of two opposing lipid bilayers, were then calculated by the Bragg law. The nature of the short-range lipid conformation was derived analyzing the high-angle X-ray diffraction profiles, being characteristic of the lipid chain organization.

2.10. Biodistribution studies of ^{99m}Tc-NLCs

Animal experiments were carried out in compliance with the relevant national laws relating to the conduct of animal experimentation and in accordance with EC Directive 86/609/EEC for animal experiments. Each biodistribution study has been acquired in tomographic mode with the YAP-(S)-PET small animal scanner prototype [26]. Healthy (fe)male Wistar rats weighing 100-150 grams were anesthetized with an intramuscular injection of a mixture of ketamine (80 mg/kg) and xylazine (19 mg/kg) and then a ^{99m}Tc-NLC dispersion was administered by different routes, namely: i.p., i.v., i.n. or per os. The administered volumes and the activity for each in vivo experiment are reported in Table 1. The SPECT whole-body studies were acquired at different time points after the injection, with the initial tomographic acquisition starting nearly 15 min after the injection. Each SPECT whole-body acquisition consisted of 3 bed positions 36 mm apart, 20 min for each position, 128 views over 360°. The SPECT cerebral studies were acquired starting 6 h after the injection, and the acquisition consisted of 1 bed position, 120 min, 128 views over 360°. The used energy window is 140−250 keV and the images were reconstructed by using the iterative EM-ML algorithm including the collimator response. CT images have been acquired, at the end of biodistribution studies, using the digital X-ray imaging system integrated into the YAP(S)PET scanner [28]. Acquisition parameters for X-ray projections were: X-ray tube voltage = 35 kV, anode current = 1 mA, exposure = 1 s, 64 views over 360°, magnification factor = 1.2. Subtraction of dark noise contribution and flat field corrections were accomplished to obtain final images. The CT data were reconstructed by using the FDK algorithm. Amide software [29] has been used for images registration, visualization and analysis.

3. Results and Discussion

The main object of this study was the production of radiolabeled NLC as new tool for imaging and biodistribution studies. To this aim, the neutral bis(dithiocarbamate) nitrido ^{99m}Tc complex, containing a terminal ^{99m}Tc≡N multiple bond (such as [^{99m}Tc]N-DBODC$_2$), was suitably synthesized, included in NLC, characterized and later employed as tracer for biodistribution studies by SPECT analyses [22,30].

3.1. Preparation of ^{99m}Tc complex

[^{99m}Tc]N-DBODC$_2$ is a neutral lipophilic symmetrical compound that was produced through the two-step synthesis schematized in Fig. 1. The complex possesses a square pyramidal geometry with an apical ^{99m}Tc≡N multiple bond and the two dithiocarbamate ligands spanning the residual four positions on the square plane through the four sulfur atoms of the two >CS$_2$ groups.

The radiochemical purity was > 95% as determined by chromatographic methods. The [^{99m}Tc]N-DBODC$_2$ complex was purified from excess of the reagents using the procedure reported in the experimental section. Approximately 80% of the activity was collected in 1mL of EtOH.

The chemical structure of the [^{99m}Tc]N-DBODC$_2$ complex was determined by chromatographic comparison with the corresponding complex prepared and characterized with the long-lived isotope ^{99m}Tc at the macroscopic level (millimolar concentration) (data not shown).

3.2. Preparation of ^{99m}Tc-NLCs

In order to obtain reliable results from the biodistribution analysis of nanoparticle by SPECT, it is important to employ radiolabeled nanoparticles resembling, as strictly as possible, their non-radiolabeled counterparts that will be effectively used in therapy.

Therefore, in the current study, a preliminary and accurate analysis of the effect of the inclusion of the [^{99m}Tc]N-DBODC$_2$ complex (used as radioactive tracer) on the dimensional and morphological characteristics of the produced NLCs was preliminarily performed.

In this respect, it is to be noted that for the inclusion of [^{99m}Tc]N-DBODC$_2$ in NLCs, the addition of at least 1 ml of EtOH to the melted LP is mandatory, due to the fact that the [^{99m}Tc]N-DBODC$_2$ complex is indeed formed in EtOH.

Therefore, a set of experiments was performed in order to determine if the addition of ethanol or [^{99m}Tc]N-DBODC$_2$ in solution could result in modifications of the NLC characteristics. In order to facilitate reading, throughout the text, the abbreviations used to indicate the different lipid nanoparticles, together with the composition of nanoparticles, are reported in Table 2.

The macroscopic analysis of the obtained nanoparticle demonstrated that the general aspect of NLC dispersions prepared in the absence or in the presence of ethanol (used for [^{99m}Tc]N-DBODC$_2$ solubilization) was very similar, with a homogeneous milky appearance (Fig. 2). Notably, in all preparations the presence of a small amount of solid lipids, in form of a floating flat layer, was evident. This presence was attributed to a partial coalescence of the LP droplets, during cooling process (see Fig. 2). In order to quantify the loss of lipids (due to coalescence), the floating flat layer was accurately weighted, after collection by small tweezers; notably, in all preparations, the lipid loss was very limited and generally comprised between 5 and 7 % (w/w), as reported in Table 2, with no appreciable differences among C-NLC, EtOH-NLC and ^{99m}Tc-NLC.

3.3. Characterization of NLCs

The particle size characterization has a paramount importance for evaluating the stability of colloidal systems and it is a fundamental parameter for quality control. Notably, size distribution analysis represents a mandatory prerequisite to verify the suitability of the particles for in vivo administration. Indeed information about morphology, size and size distribution is particularly important since the biophysical properties strongly influence biological activity, biodistribution and toxicity [6,8,31]. Unfortunately, the complex and dynamic nature of nanoparticles perplexes their characterization, and therefore a single characterization technique is not always sufficient to obtain a deep dimensional information on nanosystems. For this reason the complementary use of more than one technique (i.e. SdFFF, PCS and microscopy) is strongly desirable to obtain reliable enlightenments about the nanoparticle characteristics and therefore its suitability as delivery system.

In this respect, the results of sizing by PCS of the various nanoparticle samples are summarized in Table 3. The table shows the z-average diameter (the mean diameter based upon the intensity of scattered light), the polydispersity index (P.I.) (an estimate of the width of the distribution) and the mean size calculated by intensity, volume and number. All the dimensional data represent the means of 3 repeated measurements made on NLC samples.

Typically, the prepared NLCs showed appropriate dimensional characteristics for an i.v. administration, with mean diameters around 190 nm and a narrow size distribution, as proved by the P.I. ranging between 0.21 and 0.25.

NLCs size distribution was also determined by SdFFF analysis. The method enables to measure the particle size distribution by retaining particles of different diameter and eluting them at a calculable time [32].

The obtained fractograms were later converted into particle size distribution plots, according to well-proven equations. Indeed since an observed retention time can be directly related by theory to the mass of the eluting particles, the retention time is transformed into a size and the UV signal into a mass frequency function [25,26].

Since particle in SdFFF are sorted based on their specific mass, knowing the particle density and by supposing a spherical shape, the sizes represent diameter of an equivalent sphere [33]. Typical particle size distribution plots of NLC samples are reported in Fig. 3.

Fig 3A, referring to C-NLCs, shows a quite narrow peak at about 70 nm and a secondary population at 140 nm, along with a 5.5% of very large particles broadly distributed, spanning between 270 nm up to 1.5 µm. The addition of ethanol caused the disappearance of the larger particles, as shown in Fig 3B. Finally Fig 3C reports the particle size distribution plot of ^{99m}Tc-NLC, where besides the narrow peak, a net shoulder at 130 nm can be noticed together with a very small population of particles at about 460 nm. SdFFF analysis evidenced that in the case of ^{99m}Tc-NLC, 70% of nanoparticle mean diameters resulted below 150 nm while this percentage was 60% and 65% for EtOH-NLC and C-NLCs respectively (data not shown).

It must be underlined that PCS and SdFFF are based on completely different principles. PCS assesses the dimension considering the diffusion of the light scattered, so results depend on the particle position when they are hit by the laser ray. For data evaluation, the spherical shape is assumed and uncertainties may result from non-spherical particle shapes. In fact anisometric particles have larger diffusion coefficient than spheres of the same volume, so for anisometric particles a larger hydrodynamic diameter can be

observed by PCS. On the other hand SdFFF in some extent "weighs" the particles since in this case they are considered as compact spheres of uniform density, thus SdFFF somewhat strengthens the mass of anisometric particles in spheres, resulting in this way in smaller dimensional values with respect to PCS [23,34,35]. In this respect the complementary evaluation of size distribution by PCS and SdFFF appears essential in order to obtain realistic information about particle size.

The ^{99m}Tc-NLC size (main population 130-140 nm) resulted compatible to their in vivo administration by different routes, such as i.p., i.v., per os and i.n..

3.4. NLC morphological analysis

Cryo-TEM analyses were conducted in order to shed light on the general morphology and internal structure of the dispersed particles in NLC dispersions.

Fig. 4 shows cryo-TEM images of NLCs, including samples of C-NLC (panel A) and EtOH-NLC (panel B); for comparison the image of ^{99m}Tc-NLC is also reported in panel C.

As previously reported, the use of blends of lipids in solid (i.e. tristearin) and liquid state (i.e. miglyol) lead to the formation of imperfect lipid matrix structures with the absence of clearly identifiable oil droplets in the NLC samples [8,24]. In all panels ovoid and ellipsoidal platelet-like crystalline particles and dark, "ufo-like" structures edge-on viewed can be observed [35-37].

No significant differences are appreciable between A-C panels, indicating that the presence of EtOH and of [^{99m}Tc]N-DBODC$_2$ did not affect the NLC aspect.

3.5. X-ray diffraction measurements

Fig. 5 shows the X-ray diffraction results for samples of C-NLCs, EtOH-NLC and of ^{99m}Tc-NLC, from bottom to up.

The very similar X-ray diffraction profiles confirmed that the inner structure of all NLCs was identical. In particular, one (or two) Bragg peaks were observed in the low angle region: peak spacings suggested a lamellar structure, and the long dotted lines indicated that unit cell dimension was the same in all the considered cases. Indeed, unit cell was 446 nm, as already detected in nanoparticulate lipid dispersions used for bromocriptine delivery [24].

At high-angle diffraction, two sharp peaks were evident in all preparations. As a result, an ordered nature of the hydrocarbon chains inside the lamellae can be suggested.

Noticeable is the fact that the detected peaks were centered in the same position, endorsing that the presence of EtOH and/or [^{99m}Tc]N-DBODC$_2$ did not alter the NLC structure.

3.6. Loading efficiency of [^{99m}Tc]N-DBODC2 in NLCs and stability studies

With respect to biodistribution studies, it should be underlined that some authors have studied the body distribution of lipid nanoparticle in rats by scintigraphy, but in such studies the ^{99m}Tc complexes were loaded into NLCs after their preparation, by incubating the NLC suspension with a solution containing the ^{99m}Tc complexes, for 10-30 min at room temperature [38,39]. These methods were questionable since they did not assure the radiotracer to be stably associated into the lipid matrix both in vitro and after in vivo administration. By contrast, in our study the loading of the radioactive tracer was achieved during NLC production by a specifically designed procedure that lead to the formation of a stable complex between the tracer and nanoparticles (i.e. by addition of an EtOH solution of [^{99m}Tc]N-DBODC$_2$ to the melted lipids), allowing the inclusion of the ^{99m}Tc complex into the lipid matrix of NLCs. Notably, the encapsulation of the ^{99m}Tc complex into NLCs was highly satisfactory both in term of RCP (greater than 95%) and encapsulation efficiency. The radiolabelling was indeed almost quantitative as proved by the fact that the whole activity was within nanoparticle matrix. The high encapsulation efficiency was attributed to the stable association (solubilization) of the [^{99m}Tc]N-DBODC$_2$ complex into the melted lipids during NLC preparation.

Preliminary stability studies were performed in vitro before in vivo biodistribution studies; it is indeed important, for any biodistribution study, to assess if the imaged radioactivity is due to labelled particles or to the label only. To this aim, the ^{99m}Tc-NLC were incubated in rat serum for different lenghts of time in order to verify if in such conditions all the radioactivity would remain associated to the nanoparticle. The stability of ^{99m}Tc-NLC was determined by TLC up to 6 hours from the preparation. The TLC analysis, reported in Fig. 6, clearly shows that all labelling ^{99m}Tc-DBODC$_2$ compound remain associated to the nanoparticles, displaying a value of R_f equal to 0. Notably, in the same chromatographic conditions, the free ^{99m}Tc-DBODC$_2$ shows a completely different R_f (equal to 0.42).

3.7. Biodistribution studies of ^{99m}Tc-NLC in rats

Many papers evaluating NLC as a drug carrier have focused on the release of the NLC encapsulated drug without analysing the distribution of the NLC carrier itself. Knowing the biodistribution of the carrier is especially important in designing the appropriate NLC composition (i.e. in term of lipid and/or surfactants constituents) to control drug (passive) targeting behavior after administration through different routes.

SPECT studies can be considered as a valid alternative to ex vivo counting or autoradiography, especially in the case of research fields in which new radiopharmaceuticals have to be evaluated in small animals before clinical use or in which the investigation of molecular mechanisms of disease is performed by transgenic and knockout mice [19]. Due to the size of the animals involved, the imaging devices require specific spatial resolution and sensitivity in subjects ten or more times smaller than humans [19]. Employing well established mathematical processing, quantitative analysis of the collected images can be performed, allowing a precise determination of the radioisotope concentration in specific animal body regions, with a detection limit down to 1.34 MBq [20].

In the present study SPECT has been employed as a new technique to investigate nanoparticle biodistribution, resulting in very higher resolution images with respect to many papers employing different techniques [18,38,39].

Fig. 7 shows the ^{99m}Tc-NLC distribution after the i.p. injection. During the 1st hour the intestine and urinary tract showed a high uptake, while the liver showed a lower activity concentration. In the following 3 hours the activity concentration in the liver showed an increase, while the intestine level was near stable. Starting from the 2nd hour, a small region in the rat back showed a visible uptake, such region was identified as the “corpus adiposum nuchae” (CAN) in the rat’s interscapular area [40]. This region was described as the principal depot of brown adipose tissue in the rodents. Brown adipose tissue, that in humans is located in the supraclavicular area, has largely been studied for its role in thermogenesis and in controlling energy homeostasis [41,42].

In the present investigation the presence of NLC accumulated in CAN was attributed to a tropism of lipid nanoparticles for adipose tissue. Fig. 8 better highlights the CAN region viewed by trans-axial, coronal and sagittal images.

Fig. 9 shows the ^{99m}Tc-NLC distribution after the i.v. injection. As expected, in this case the liver evidenced a remarkable uptake, that is clearly visible in all images. Also for i.v. administration, during the 1st hour ^{99m}Tc-NLC were consistently accumulated in CAN, while the activity concentration in this region progressively decreased in the following three

hours. Starting from 2nd hour the intestine tract showed a progressive uptake, up to reach a radioactivity level comparable with that of liver. The high level of radioactivity in the liver can be attributed to the discontinuous liver endothelium, offering a passage for ^{99m}Tc-NLC as hypothesized by Beloqui and colleagues [16]. The radioactivity observed in the intestine was a result of the fragmentation of NLC in the liver, leading to release of radioactivity through the bile duct, as suggested by Andreozzi and colleagues [43]. Particularly the tropism of NLC for CAN achieved by i.p. and i.v. routes represents an important finding. At the best of our knowledge, no other descriptions of this accumulation has been yet reported in literature. This topic deserves to be highly considered since it has been demonstrated that the activation of thermogenesis by brown adipose tissue results in an increasing whole-body expenditure and regulation of adiposity, offering new therapeutics to treat human obesity [42]. In this respect, our study demonstrated that NLC can efficiently reach, probably by passive targeting, the brown fat tissue. The administration of NLC containing specific brown fat activators could represent a therapeutic strategy in the treatment of human obesity and related metabolic disorders.

Fig. 10 shows ^{99m}Tc-NLC distribution after per os administration. The images report the main uptake in the intestine tract. When ^{99m}Tc-NLCs were administered per os, they were probably taken up by the gastro-intestinal tract and transferred to the reticulum-endothelial organs. This result confirms previous findings, indicating that NLC are rapidly cleared from the systemic circulation by opsonization and uptake by the reticulum-endothelial system [14,15]. In particular NLC mainly accumulated in the liver and were adsorbed within the small intestine [44].

Fig. 11 shows the ^{99m}Tc-NLC distribution after the i.n. administration. The images evidence that the activity distribution remained in the nose.

The absence of radioactivity in the brain suggests that NLC did not reach this organ by any administration route employed in the present study, comprising the i.n. one, in contrast to results reported by other authors [38,39,45].

Taken together, the obtained images demonstrated that NLC distributed mainly in the liver after i.p. and i.v. administration and in the intestine by oral and i.v. route.

It should be underlined that the free ^{99m}Tc-$DBODC_2$ has a particular tropism for myocardial tissue when in vivo administered [30,46]. This particular labelling compound has been indeed selected to take advantage from its peculiar in vivo biodistribution.

Thanks to the particular biodistribution profile of the free labelling compound, it is indeed possible to unequivocally discern between the signal given by the radiotracer

encapsulated into nanoparticles and that of the free labelling compound. If even small amount of the labelling compound would have been leaked out form the nanoparticles, a clear heart associated signal would have been appeared. In this respect the absence of any accumulation of radioactivity in the cardiac tissue is a unequivocal proof of the fact that the radioactive signal is due to ^{99m}Tc-NLC.

As proved by the SPECT images reported in Figs. 7-10, the absence of radioactivity in the heart clearly indicated that labelling compound was completely and firmly associated to NLC. At this regard, it is to be emphasized that the absence of heart signal, up to 6 hours from the administration, indicated that NLC remained stable in vivo, suggesting the suitability of NLC as controlled release formulation for drugs and radiochemical for therapeutic as well diagnostic purposes.

4. Conclusions

In the present investigation an efficient strategy to obtain radiolabeled nanoparticles suitable for biodistribution study has been reported. To this aim, the inclusion of ^{99m}Tc-$DBODC_2$ in NLC was described, showing that the presence of the radioactive label does not affect the morphology and dimension of nanoparticles.

The employed YAP-(S)-PET small animal scanner prototype enabled to evaluate the biodistribution of ^{99m}Tc-NLC, collecting high-quality scintigraphic images. The images clearly indicate that nanoparticles, after i.p., i.v. and per os administration, are present (even if in different extents) in liver and intestine. The absence of radioactivity in myocardial tissue confirmed that the described protocol was suitable to firmly include the radiotracer ^{99m}Tc within the nanoparticles.

Taken together the results described in the current paper present a number of innovative aspects, as below described.

a) SPECT represents an innovative technique to study lipid nanoparticle biodistribution, resulting in very high resolution images with respect to other techniques recently described [18,38,39].

b) A procedure able to firmly encapsulate the radiotracer within nanoparticles has been described; this aspect appears to be particularly important when compared to other papers describing the association of labels to nanoparticles, without controlling the stability of the tracer-nanoparticle complex.

c) The selection of the specific ^{99m}Tc-DBODC$_2$ as radiotracer for nanoparticles gave the opportunity to have an internal control for assuring the stability of the tracer-nanoparticle complex. As previously discussed, even limited amounts of free labelling radiotracer can be detected.

d) Finally, thanks to the high resolution images obtained by SPECT, it was possible to detect the nanoparticle presence in brown fat tissue. This finding opens up the possibility to propose NLC as potential delivery system for molecules resulting in beneficial effect for obesity treatments and related metabolic disorders.

Acknowledgments

This work was funded by "FIRB 2010. Fondo per gli Investimenti della Ricerca di Base" from the Ministry of the University and research of Italy. Thanks are given to Dr L.M. Feggi (Unit of Nuclear Medicine, S. Anna Hospital, Ferrara, Italy) for equipment.

References

[1] A. M. Nyström, B. Fadeel, Safety assessment of nanomaterials: Implications for nanomedicine. J.Control. Release 161 (2012) 403-408**.**

[2] R. A. Petros, J. M. De Simone, Strategies in the design of nanoparticles for therapeutic applications. Nat. Rev. Drug. Discov. 9 (2010) 615-627**.**

[3] L. Zhang, F.X. Gu, J. M. Chan, A. Z. Wang, R. S. Langer, O. C. Farokhzad, Nanoparticles in Medicine: Therapeutic Applications and Developments. Clin. Pharmacol. Ther. 83 (2008) 761-769**.**

[4] N. Sanvicens, M. P. Marco, Multifunctional nanoparticles–properties and prospects for their use in human medicine. Trends Biotechnol. 26 (2008) 425-433**.**

[5] M.D. Joshi, R. H. Müller, Lipid nanoparticles for parenteral delivery of actives, Europ. J. Pharm. Biopharm. 71 (2009) 161-172.

[6] S.A. Wissing, O. Kayser, R.H. Muller, Solid lipid nanoparticles for parenteral drug delivery, Adv. Drug Delivery Rev. 56 (2004) 1257-1272**.**

[7] W. Mehnert, K. Mader, Solid lipid nanoparticles, production, characterization and applications, Adv. Drug Delivery Rev. 47 (2001) 165-196**.**

[8] A. Saupe, S. A. Wissing, A. Lenk, C. Schmidt, R. H. Müller, Solid Lipid Nanoparticles (SLN) and Nanostructured Lipid Carriers (NLC) - Structural investigations on two different carrier systems, Bio-Med. Mater. Eng. 15 (2005) 393-402**.**

[9] S.S. Shidhaye, R. Vaidya, S. Sutar, A. Patwardhan, V.J. Kadam, Solid lipid nanoparticles and nanostructured lipid carriers-innovative generations of solid lipid carriers, Curr. Drug Deliv. 5 (2008) 324-331**.**

[10] G. Yoon, J.W. Park, I.-S. Yoon, Solid lipid nanoparticles (SLNs) and nanostructured lipid carriers (NLCs): recent advances in drug delivery, J. Pharm. Investig. 43 (2013) 353-362.

[11] M. Joshi, V. Patravale, Nanostructured lipid carrier (NLC) based gel of celecoxib, Int. J. Pharm. 346 (2008) 124-132.

[12] A. Puri A, K. Loomis, B. Smith, J.H. Lee, A. Yavlovich, E. Heldman, R. Blumenthal, Lipid-based nanoparticles as pharmaceutical drug carriers: from concepts to clinic, Crit. Rev. Ther. Drug Carrier Syst. 26 (2009) 523-580**.**

[13] L. Battaglia, Gallarate, Lipid nanoparticles: state of the art, new preparation methods and challenges in drug delivery, Expert Opin. Drug Deliv. 9 (2012) 497-508.
[14] M.A. Iqbal, S. Md, J.K. Sahni, S. Baboota, S. Dang, J. Ali, Nanostructured lipid carriers system: Recent advances in drug delivery, J. Drug Target. 20 (2012) 813-830.
[15] J.P.M. Almeida, A.L Chen, A. Foster, R. Drezek, In vivo biodistribution of nanoparticles. Nanomedicine 6 (2011) 815-835.
[16] A. Beloqui, M.A. Solinís, A. Delgad, C. Évora, A. del Pozo-Rodríguez, A. Rodríguez-Gascón, Biodistribution of Nanostructured Lipid Carriers (NLCs) after intravenous administration to rats: Influence of technological factors, Eur. J. Pharm. Biopharm. 84 (2013) 309-314.
[17] S. Hirsjärvia, L. Sancey, S. Dufort, C. Belloche, C. Vanpouille-Box, E. Garciona, J.-L. Coll, F. Hindréa, J.-P. Benoît, Effect of particle size on the biodistribution of lipid nanocapsules: Comparison between nuclear and fluorescence imaging and counting, Int. J. Pharm. 453 (2013) 594-600.
[18] S. Ballot, N. Noiret, F. Hindré, B. Denizot, E. Garin, H. Rajerison, J.-P. Benoit, ^{99m}Tc/^{188} Re-labelled lipid nanocapsules as promising radiotracers for imaging and therapy: formulation and biodistribution, Eur. J. Nucl. Med. Mol. Imaging 33 (2006) 602-607.
[19] G. Di Domenico, G. Zavattini, in: International Atomic Energy Agency, Vienna (Ed.) Advances in spect instrumentation (including small animal scanners). Technetium-99m radiopharmaceuticals: status and trends. IAEA radioisotopes and radiopharmaceuticals series No. 1, Austria, 2009, pp: 57-90.
[20] G. Di Domenico, G. Zavattini, E. Moretti, A. Piffanelli, M. Giganti, A. Motta, N. Sabba, L. Uccelli, E. Benini, A. Duatti, C. Bolzati, A. Boschi and A. Del Guerra.,YAP-(S)PET small animal scanner: quantitative results, IEEE Transact. Nucl. Sci. 50 (2003) 1351-1356.
[21] A. Del Guerra, A. Bartoli, N. Belcari, D. Herbert, A. Motta, A. Vaiano, G. Di Domenico, N. Sabba, E. Moretti, G. Zavattini, M. Lazzarotti, L. Sensi, M. Larobina, L. Uccelli, Performance evaluation of the fully engineered YAP-(S)PET scanner for small animal imaging, IEEE Trans. Nucl. Sci. 33 (2006) 1078-1083.
[22] C. Cittanti, L. Uccelli, M. Pasquali, A. Boschi, C. Flammia, E. Bagatin, M. Casali, M.G. Stabin, L. Feggi, M. Giganti, A. Duatti, Whole-Body Biodistribution and Radiation Dosimetry of the New Cardiac Tracer ^{99m}Tc-N-DBODC, Journal of Nuclear Medicine. 49, 8 (2008) 1299-1304.

[23] R. Pecora, Dynamic Light Scattering Measurement of Nanometer Particles in Liquids, J. Nanoparticle Res. 2 (2000) 123-131.
[24] E. Esposito, P. Mariani, L. Ravani, C. Contado, M. Volta, S. Bido, M. Drechsler, S. Mazzoni, E. Menegatti, M. Morari, R. Cortesi, Nanoparticulate lipid dispersions for bromocriptine delivery: characterization and in vivo study, Eur. J. Pharm. Biopharm. 80 (2012) 306-314.
[25] C. Contado G. Blo, F.Fagioli, F. Dondi, R. Beckett, Characterisation of River Po particles by sedimentation field-flow fractionation coupled to GFAAS and ICP-MS, Colloid Surface A 120 (1997) 47-59.
[26] E. Esposito, M. Fantin, M. Marti, M. Drechsler, L. Paccamiccio, P. Mariani, E. Sivieri, F. Lain, E. Menegatti, M. Morari, R. Cortesi, Solid lipid nanoparticles as delivery systems for bromocriptine, Pharm. Res. 25 (2008) 1521-1530.
[27] V. Luzzati, H. Delacroix, T. Gulik-Krzywicki, P. Mariani, R. Vargas, The cubic phases of lipids, Curr. Top. Membr. 44 (1997) 3-25.
[28] G. Di Domenico, N. Cesca, G. Zavattini, N. Auricchi, M. Gambaccini, CT with a CMOS flat panel detector integrated on the YAP(S)PET scanner for in vivo small animal imaging, Nucl. Instrum. Meth. Phys. Res. A 571 (2007) 110-113.
[29] A.M. Loening, S.S. Gambhir, AMIDE: A Free Software Tool for Multimodality Medical Image Analysis, Mol. Imaging, 2 (2003) 131-137.
[30] R. Pasqualini, A. Duatti, E. Bellande, V. Comazzi, V. Brucato, D. Hoffshir, D. Fagret, M. Comet, Bis(dithiocarbamato) nitrido technetium-^{99m} radiopharmaceuticals: a class of neutral myocardial imaging agents, J. Nucl. Med. 35 (1994) 334-341.
[31] S.U. Egelhaaf, E. Wehrli, M. Muller, M. Adrian, P. Schurtenberger Determination of the size distribution of lecithin liposomes: a comparative study using freeze fracture, cryoelectron microscopy and dynamic light scattering, J. Microsc. 184 (1996) 214-228.
[32] H.G. Merkus, Y. Mori, B. Scarlett, Particle size analysis by sedimentation field flow fractionation. Performance and application, Colloid Polym. Sci. 267 (1989) 1102-1107.
[33] H. Bunjes in: C. Nastruzzi (Ed.) Lipospheres in drug targets and delivery: approaches, methods and applications, CRC Press, New York, 2005, pp. 41-66.
[34] E. Esposito, L. Ravani, P. Mariani, C. Contado, M. Drechsler, C. Puglia, R. Cortesi, Curcumin containing monoolein aqueous dispersions: A preformulative study. Mat. Sci. Eng. C 33 (2013) 4923-4934.
[35] K. Jores, W. Mehnert, M. Drechsler, H. Bunjes, C. Johann, K. Maeder, Investigations on the structure of solid lipid nanoparticles (SLN) and oil-loaded solid lipid nanoparticles by

photon correlation spectroscopy, field-flow fractionation and transmission electron microscopy, J. Control. Release 95 (2004) 217-227.

[36] E. Esposito, L. Ravani, C. Contado, A. Costenaro, M. Drechsler, D. Rossi, E. Menegatti, A. Grandini, R. Cortesi, Clotrimazole nanoparticle gel for mucosal administration, Mat. Sci. Eng. C, 33 (2013) 411-418.

[37] E. Esposito, M. Drechsler, R. Cortesi, Microscopy characterisation of micro- and nanosystems for pharmaceutical use, OA Drug Design & Delivery 1 (2013) 2.

[38] V. Kakkar, A. K. Mishrab, K. Chuttani, I. P. Kaur, Proof of concept studies to confirm the delivery of curcumin loaded solid lipid nanoparticles (C-SLNs) to brain, Int. J. Pharm. 448 (2013) 354-359.

[39] S. Patel, S. Chavan, H. Soni, A.K. Babbar, R. Mathur, A.K. Mishra, K. Sawant, Brain targeting of risperidone-loaded solid lipid nanoparticles by intranasal route, J. Drug Targeting 19 (2002) 468-474.

[40] V. Komarek, in: G.J. Krinke (Ed.) The Laboratory Rat, Academic Press Publisher, Salt Lake City, USA, 2000, pp. 253-275.

[41] S. Kajimura, M. Saito, A new era in brown adipose tissue biology: molecular control of brown fat development and energy homeostasis, Annu. Rev. Physiol. 76 (2014) 13.1-13.25.

[42] O. Boss, S.R. Farmer, Recruitment of brown adipose tissue as a therapy for obesity-associated diseases Frontiers endocrynol. 3 (2013) 118-123.

[43] E. Andreozzi, J.W. Seo, K. Ferrara, A. Louie, A novel method to label solid lipid nanoparticles (SLNs) with 64Cu for positron emission tomography (PET) imaging, Bioconjug Chem. 22 (2011) 808-818.

[44] S. Yang, J. Zhu, Y. Lu, B. Liang, C. Yang, Body distribution of camptothecin solid lipid nanoparticles after oral administration, Pharm. Res. 16 (1999) 751-757.

[45] M. I. Alam, S. Baboota, A. Ahuja, M. Ali, J. Ali, J. K. Sahni, Intranasal infusion of nanostructured lipid carriers (NLC) containing CNS acting drug and estimation in brain and blood, Drug Delivery 20 (2013) 247-251.

[46] A. Boschi, L. Uccelli, C. Bolzati, A. Duatti, N. Sabba, E. Moretti, G. Di Domenico, G. Zavattini, F. Refosco, M. Giganti, Synthesis and biologic evaluation of monocationic asymmetric ^{99m}Tc-nitride heterocomplexes showing high heart uptake and improved imaging properties, J. Nucl. Med. 44 (2003) 806-814.

Figure Legends

Figure 1. Scheme of the two-step synthesis used for the preparation of the [^{99m}Tc]N-DBODC$_2$ neutral lipophilic symmetrical radiochemical.

Figure 2. Production of ^{99m}Tc-NLC by the 3 step procedure schematized in the figure. The lipid mixture, constituted of tristearin/miglyol plus [^{99m}Tc]N-DBODC$_2$ is melted at 80°C; an aqueous poloxamer 188 solution is added. The two phase system is high-speed stirred and subsequently ultrasonicated. After cooling at room temperature the nanoparticle suspension appears has a homogeneous milky appearance (see photograph).

Figure 3. Size distribution of lipid nanoparticles as obtained by SdFFF. Plots show the dimensional distribution of C-NLC (A), EtOH-NLC (B) and ^{99m}Tc-NLC (C).

Figure 4. Cryo-transmission electron microscopy images of C-NLC (A), EtOH-NLC (B) and ^{99m}Tc-NLC (C). Bar corresponds to 200 and 100 nm in panels A, C, E and B, D, F respectively.

Figure 5. X-ray diffraction profiles of C-NLC (○), EtOH-NLC (◊) and ^{99m}Tc-NLC (Δ).

Figure 6. Stability of ^{99m}Tc-NLC. After preparation, the nanostructured particles were incubated with rat serum and thereafter analyzed by TLC on reversed-phase C18 plates. Analyses were performed after 1 (A) or 6 hours (B) from the preparation.

Figure 7. Panel A: coronal and sagittal images of rat injected with ^{99m}Tc-NLC. SPECT in-vivo data were acquired along 1st, 2nd, 3rd and 4th hour after the intaperitoneal injection, on the right side the corresponding section of co-registered CT is shown. Panel B: tomographic coronal images of rat obtained with small-animal SPECT scanner 120 min after injection of ^{99m}Tc-NLC. Slices, taken with 1 mm spacing, are ordered as indicated by the arrows and red numbers. Color intensity is proportional to pixel activity (counts per second).

Figure 8. Tomographic trans-axial, coronal and sagittal images of rat obtained with small-animal SPECT scanner 120 min after intaperitoneal injection of ^{99m}Tc-NLC The three

images evidence the *corpus adiposum nuchae* uptake. Color intensity is proportional to pixel activity (counts per second).

Figure 9. Panel A: coronal and sagittal images of rat injected with ^{99m}Tc-NLC. SPECT in-vivo sections were acquired along 1st, 2nd, 3rd and 4th hour after the intravenous injection, on the right side the corresponding section of co-registered CT is shown. Panel B: tomographic coronal images of rat obtained with small-animal SPECT scanner 120 min after injection of ^{99m}Tc-NLC. Slices, taken with 1 mm spacing, are ordered as indicated by the arrows and red numbers. Color intensity is proportional to pixel activity (counts per second).

Figure 10. Images of rat injected with ^{99m}Tc-NLC. SPECT in-vivo coronal sections acquired 6 hours after the oral administration. In panel A slices, taken with 1 mm spacing, are ordered as indicated by the arrows and red numbers. Panel B shows the 3D rendering of biodistribution. Color intensity is proportional to pixel activity (counts per second).

Figure 11. Images of rat injected with ^{99m}Tc-NLC. SPECT in-vivo coronal sections acquired 6 hours after the nasal administration. In panel A slices, taken with 1 mm spacing, are ordered as indicated by the arrows and red numbers. Panel B shows the 3D rendering of biodistribution. Color intensity is proportional to pixel activity (counts per second).

Table(s)

Table 1. ^{99m}Tc-NLC volume, activity and acquisition type used for each administration routes.

Administration route	Injected volume [μL]	Activity injected [MBq]
Intraperitoneal	500	47
Intravenous	500	49
Oral	1000	112
Nasal	50	5

Table 2. Nanoparticle composition and production parameters

Batch identification code	Tristearin[a]	Mygliol[a]	Poloxamer 188[b]	Lipid loss[c] (%, w/w)	Notes
# C-NLC	3.35	1.65	2.63	5.2±0.1	conventional NLC
# EtOH-NLC	3.35	1.65	2.63	6.3±0.2	produced with the addition of ethanol
# Tc-NLC	3.35	1.65	2.63	6.9±0.8	produced with the addition of [^{99m}Tc]N-DBODC$_2$ solubilized in ethanol

[a]The values are expressed as weight percentage with respect to the total weight of the lipid phase.

[b]The values are expressed as weight percentage with respect to the volume of the water phase.

[c]The values are expressed as weight percentage with respect to the initial weight of the lipid phase.

Table 3. Dimensional analysis by PCS of NLCs

Parameter	C-NLC	EtOH-NLC	^{99m}Tc-NLC
Z Average	194.2	186.2	197.8
Mean diameter by intensity (nm)	191.5	179.3	184.2
Mean diameter by volume (nm)	116.5 (73.56%)* 337.4 (26.44%)*	93.4 (83.5%)* 276.3 (16.5%)*	141.4 (86.2%)* 384.4 (13.8%)*
Mean diameter by number (nm)	105.4 (98.6%)* 278.1 (1.5%)*	83.9 (98.3%)* 263.1 (1.7%)*	114.4
Polydispersity index	0.21	0.23	0.25

*Peak area

Figure(s)

Click here to download high resolution image

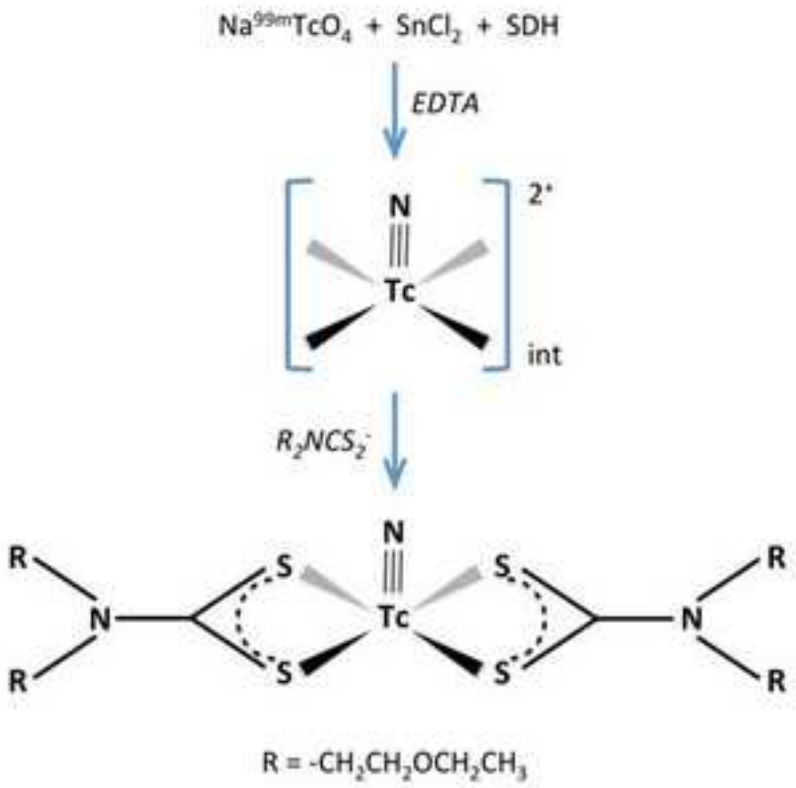

Figure 1

Figure(s)

Click here to download high resolution image

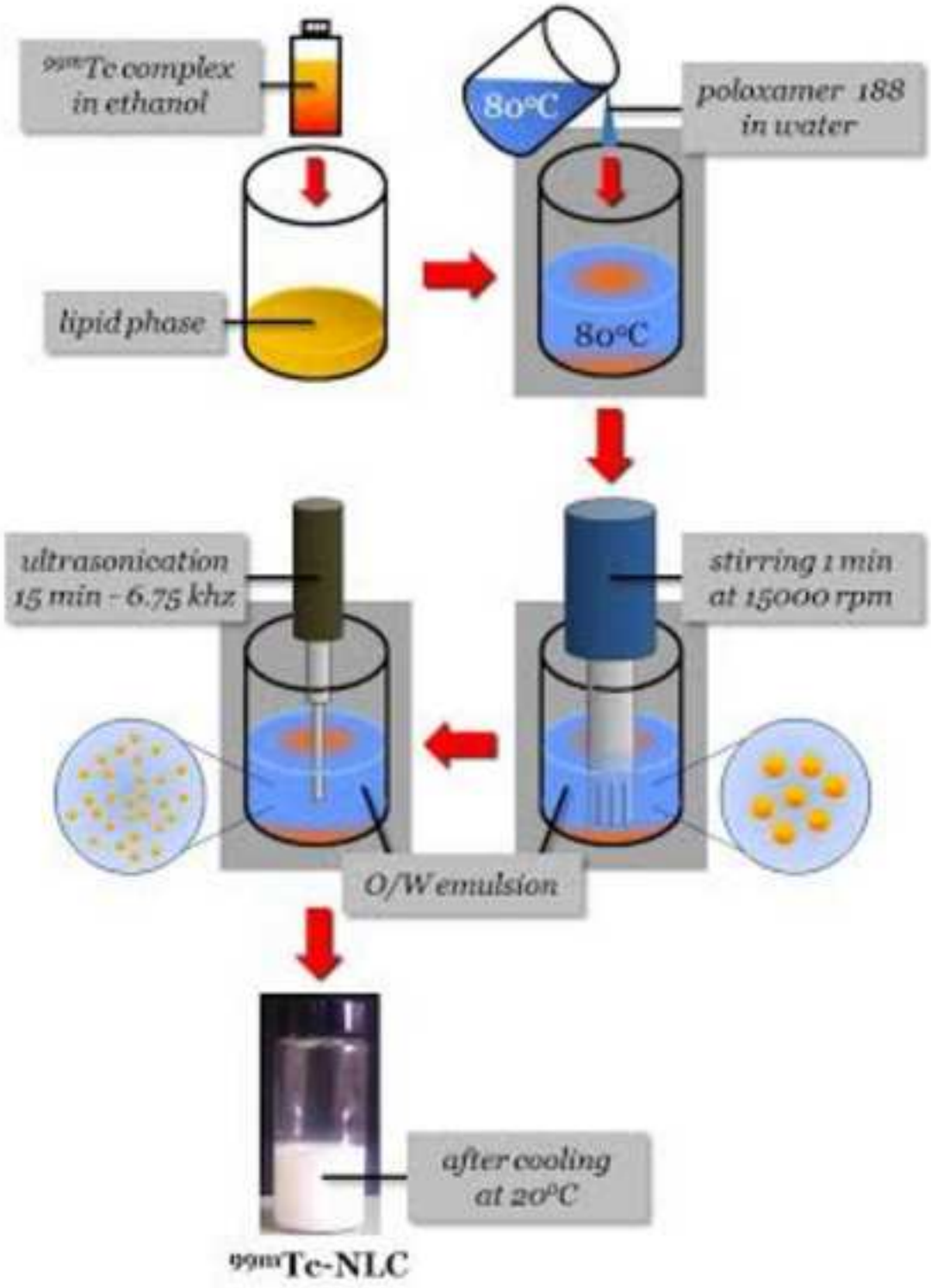

Figure 2

Figure(s)

Click here to download high resolution image

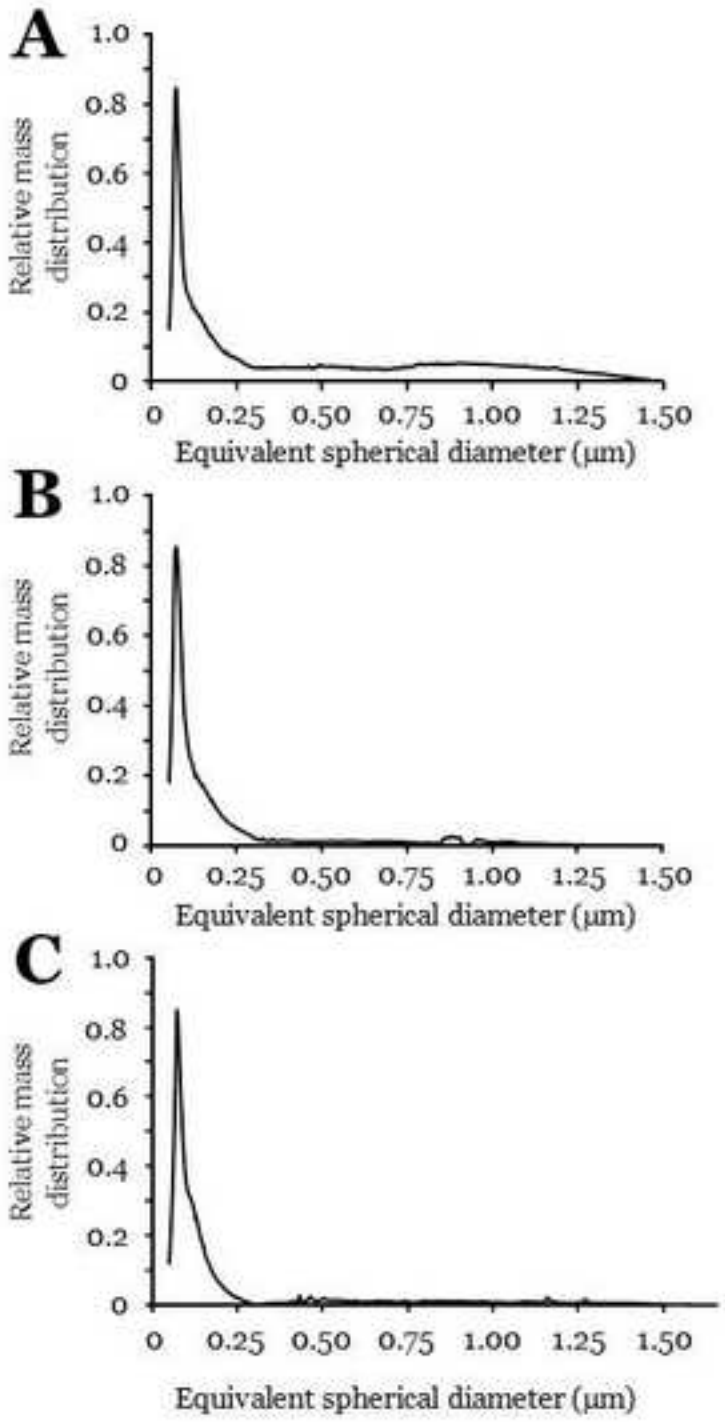

Figure 3

Figure(s)

Click here to download high resolution image

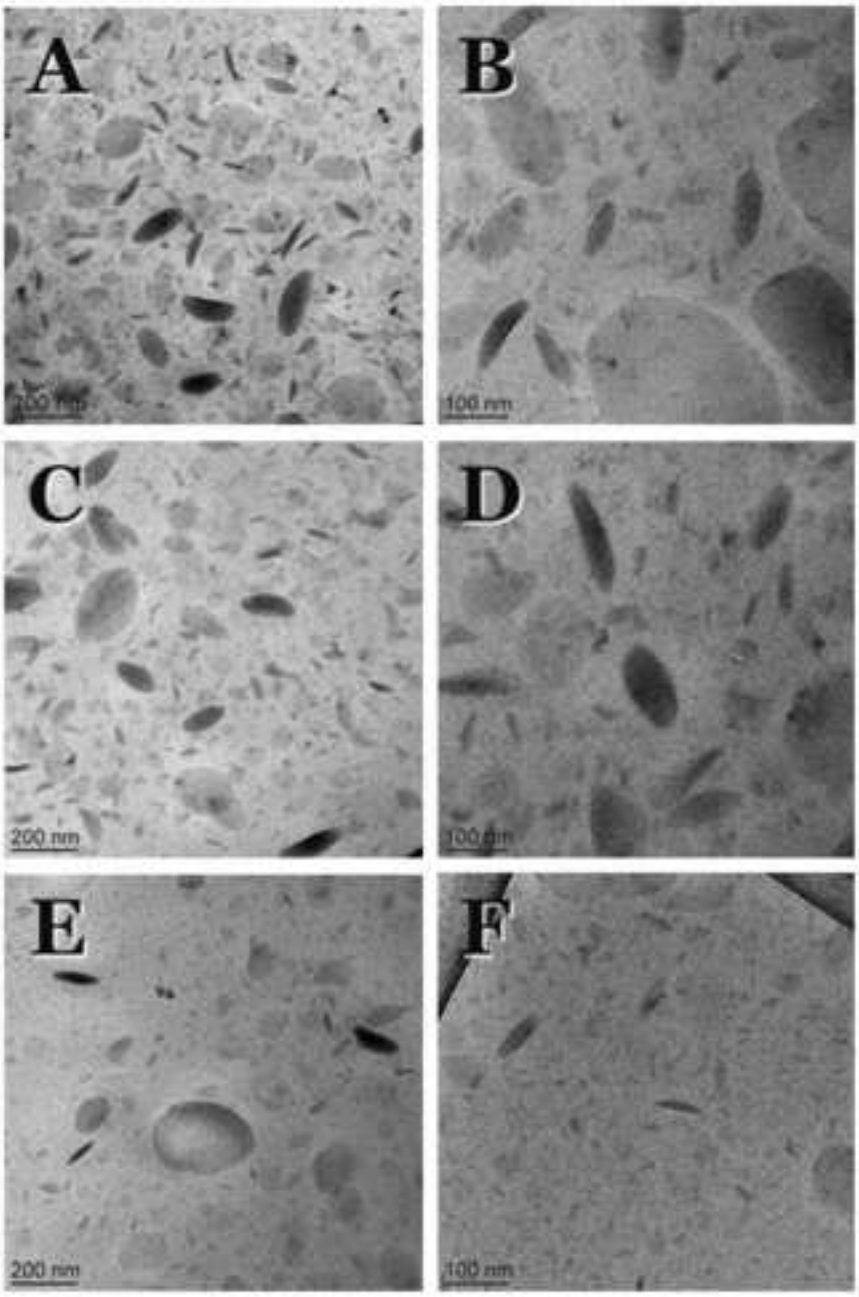

Figure 4

Figure(s)

Click here to download high resolution image

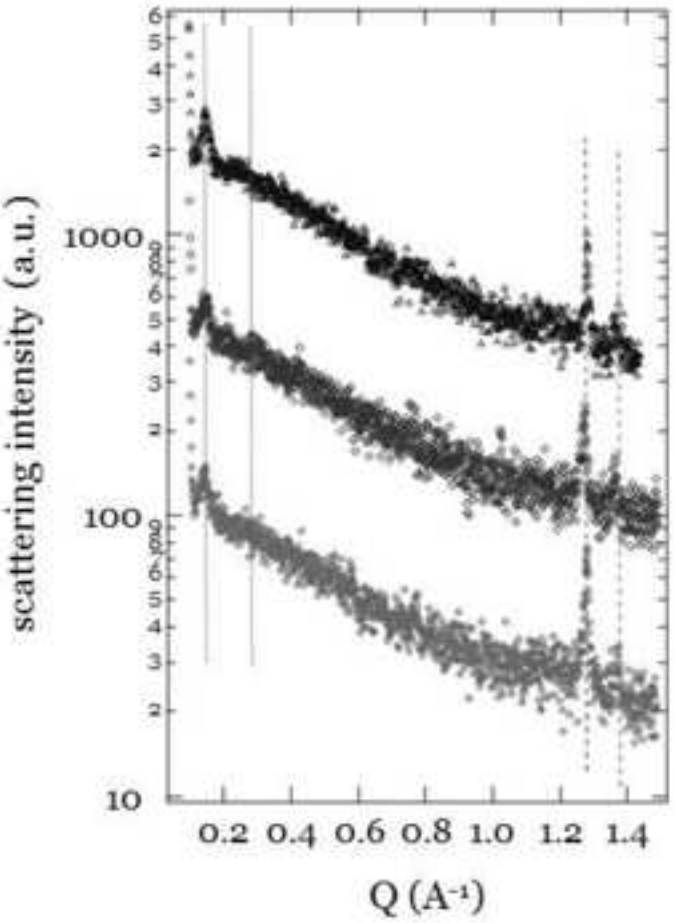

Figure 5

Figure(s)

Click here to download high resolution image

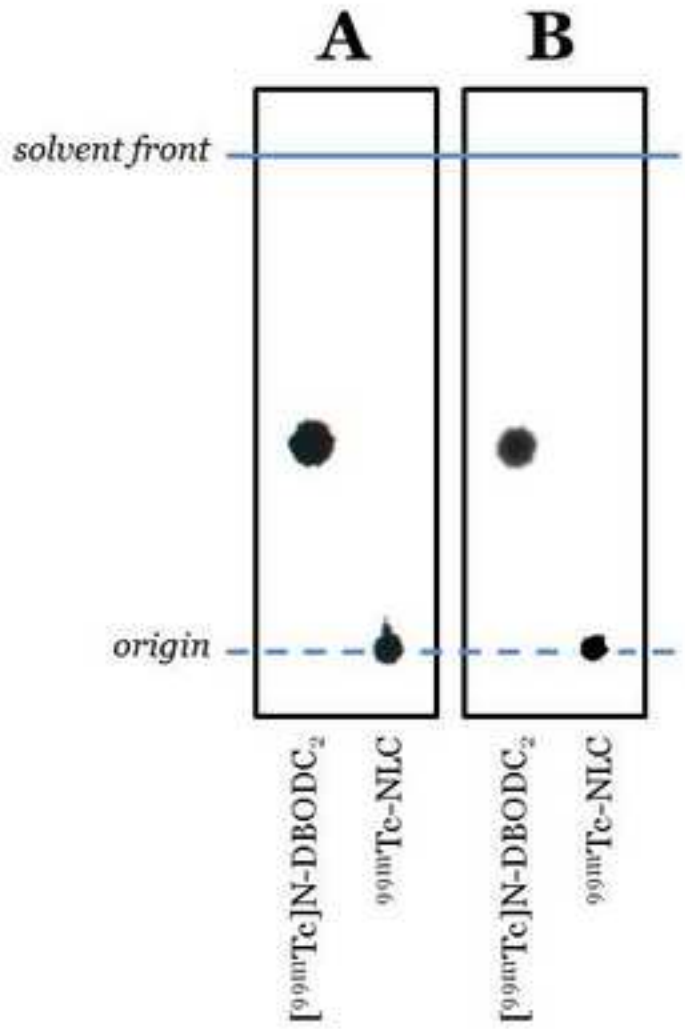

Figure 6

Figure(s)
Click here to download high resolution image

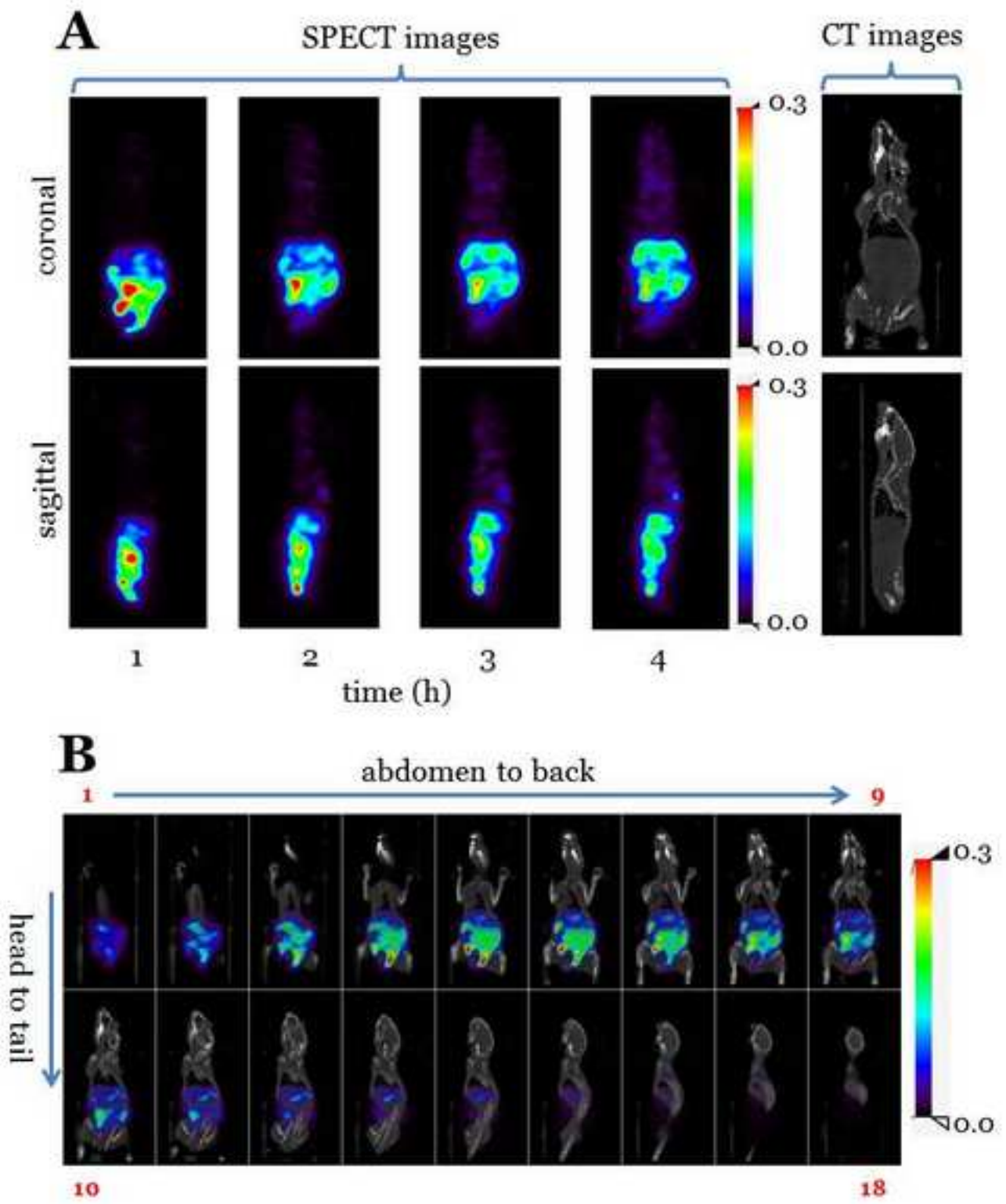

Figure 7

Figure(s)

Click here to download high resolution image

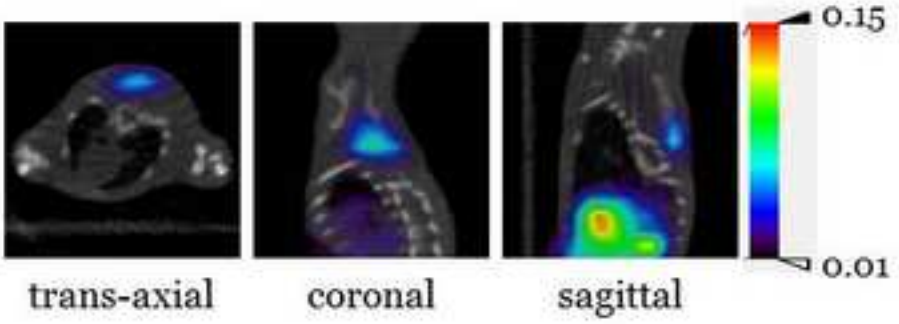

Figure 8

Figure(s)
Click here to download high resolution image

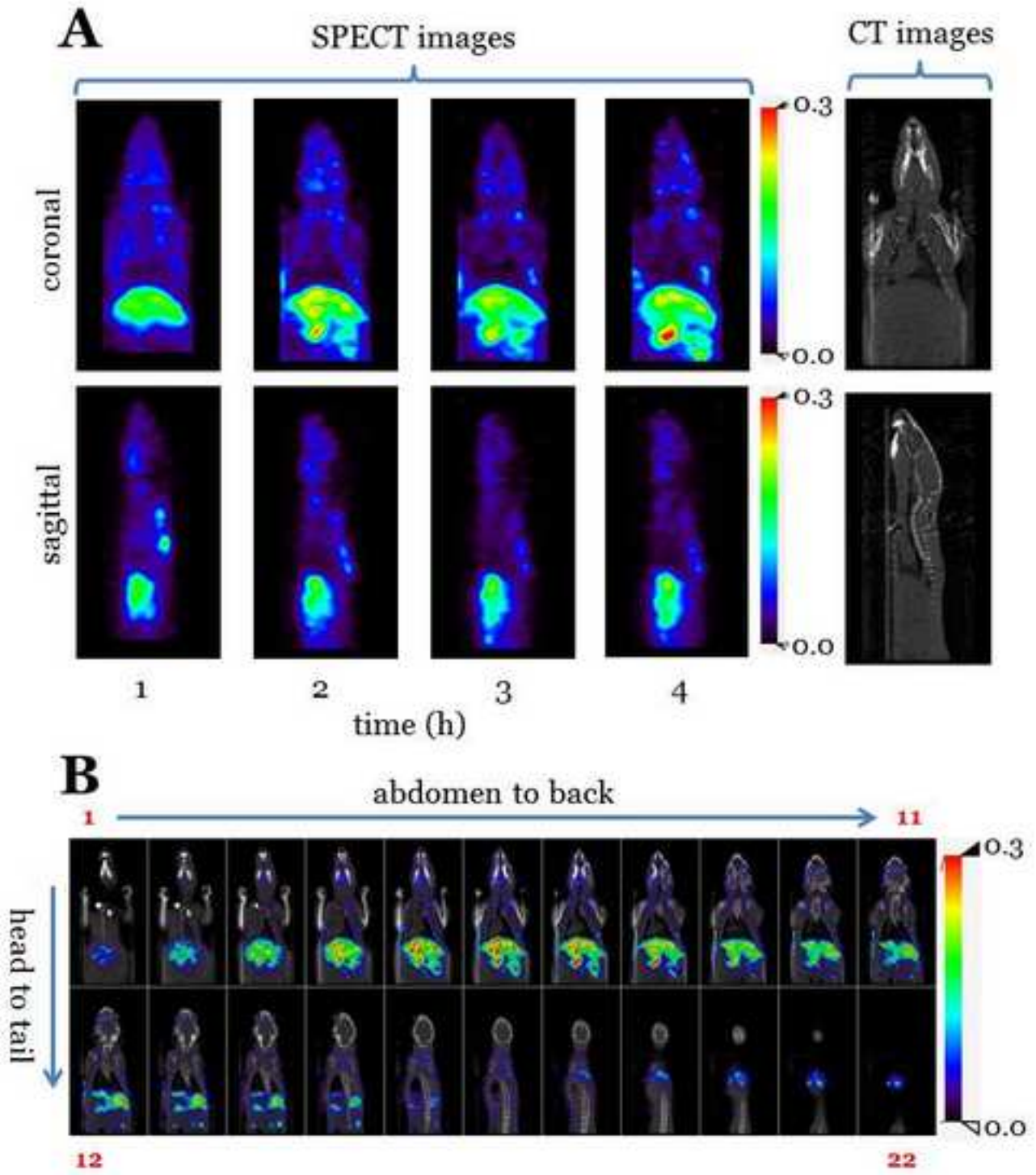

Figure 9

Figure(s)
Click here to download high resolution image

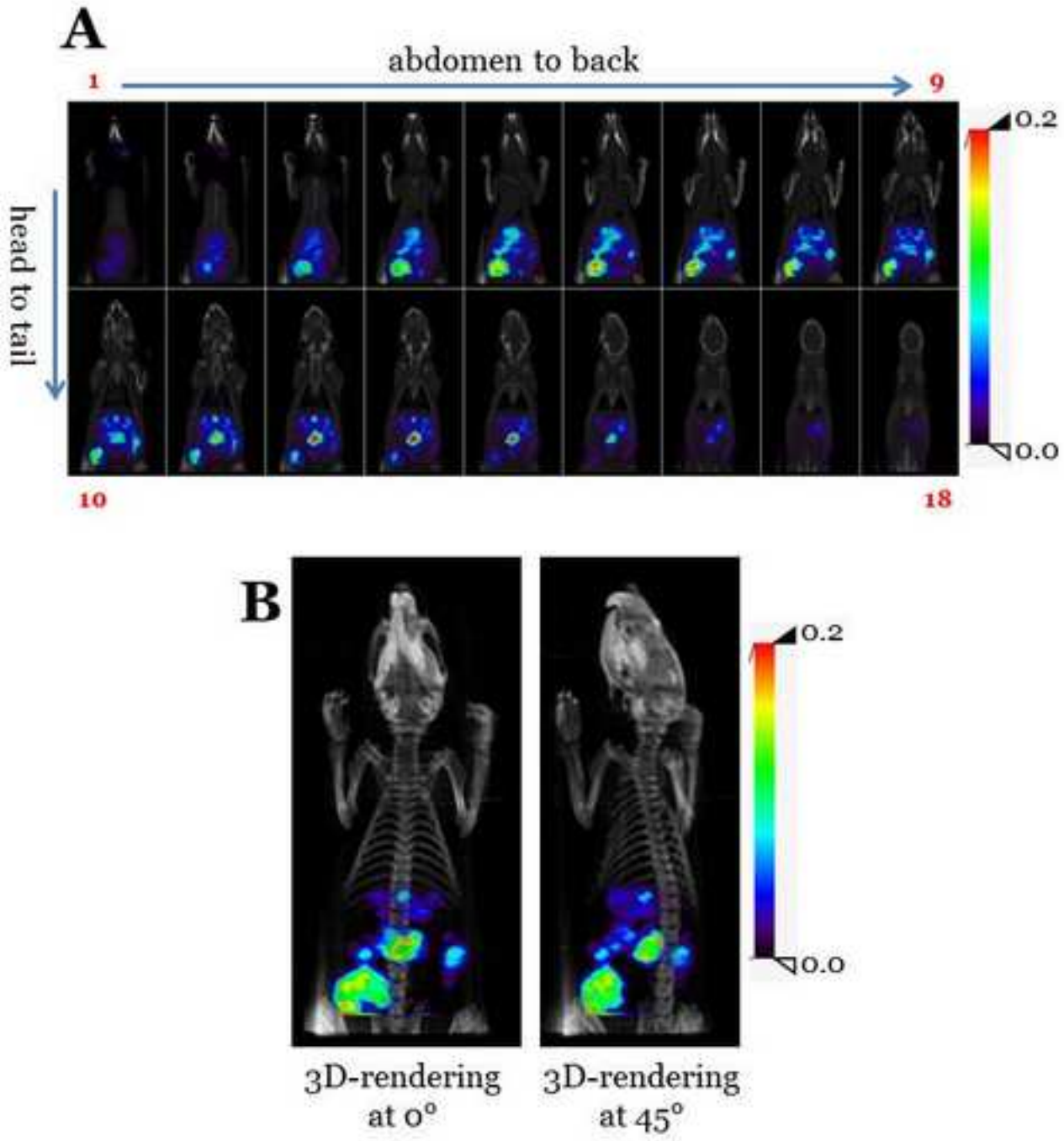

Figure 10

Figure(s)
Click here to download high resolution image

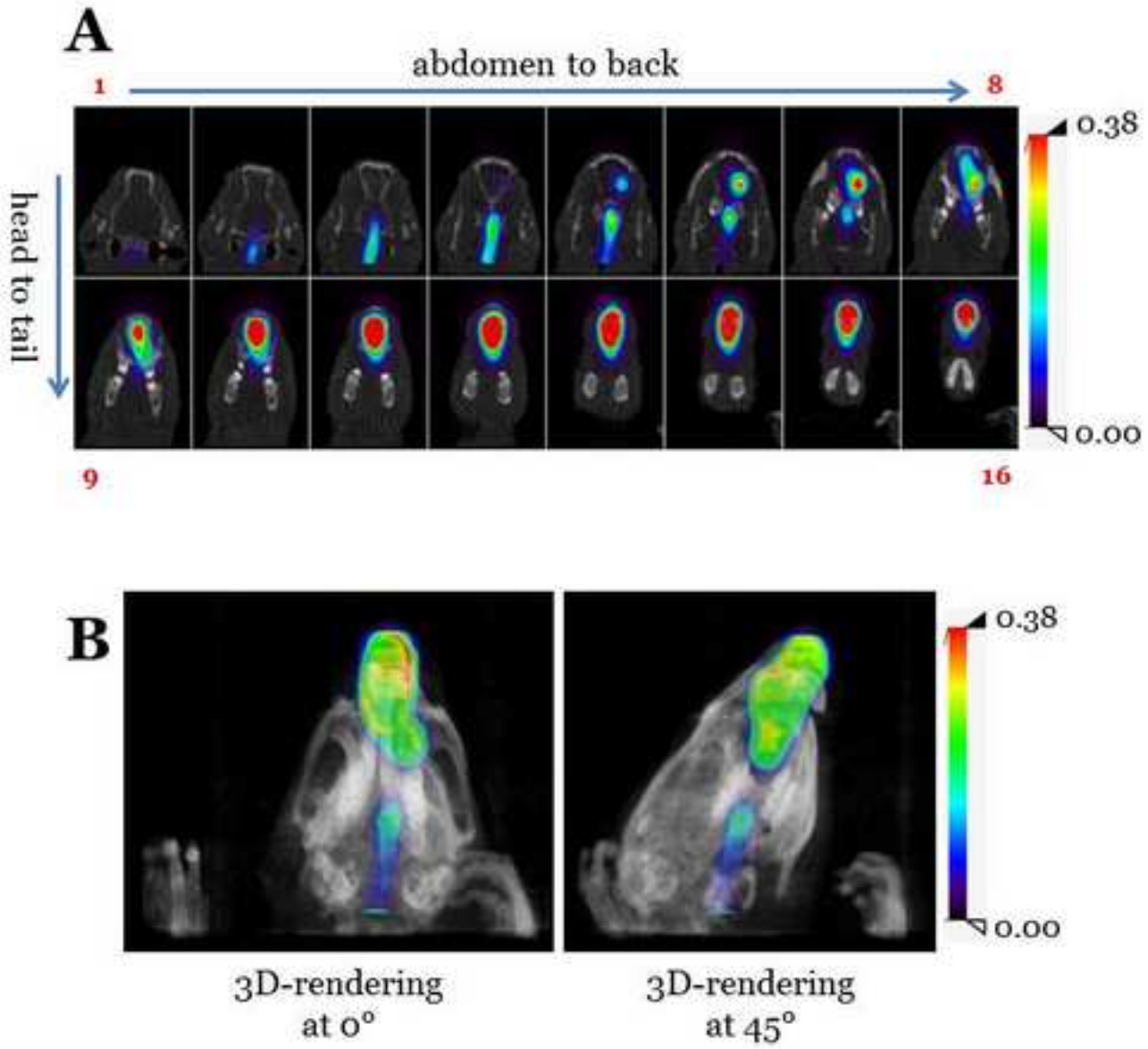

Figure 11

Abbreviations:

C-NLC: conventional nanostructured lipid carriers, prepared without the addition of EtOH; EtOH-NLC: nanostructured lipid carrier, prepared with the addition of plain EtOH; ^{99m}Tc-NLC: radiolabeled nanostructured lipid carrier, prepared with the addition of EtOH containing the [^{99m}Tc]N-DBODC$_2$ tracer; cryo transmission electron microscopy: cryo-TEM, photon correlation spectroscopy: PCS; sedimentation field flow fractionation: SdFFF; polydispersity index: P.I.; single photon emission computed tomography: SPECT; lipid phase: LP; water phase: WP; Stannous chloride dihydrate, succinic dihydrazide: SDH; ethylenediaminotetraacetic acid: EDTA; sodium salt of the bis(dithiocarbamate) ligand: DBODC; glutathione: GSH; radiochemical purity: RCP; thin-layer chromatography: TLC; ethanol: EtOH; corpus adiposum nuchae: CAN; intraperitoneal: i.p.; intravenous: i.v.; intranasal i.n.; oral: per os.